Chinese Chemical Letters 37 (2026) 111398

Contents lists available at ScienceDirect

Chinese Chemical Letters

journal homepage: www.elsevier.com/locate/cclet

Synergy of electron-trapping centers and solid adsorption toward 100% suppression of toxic byproduct N_2O in photocatalytic NO reduction

Lijun Liao[a,1], Yuhao Wang[b,1], Yanbo Li[c], Yingchun Chen[a], Ruting Yuan[a,*], Bo Wang[a], Tiancheng Zhuang[a], Guangquan Zhao[a,*], Wei Zhou[a,*]

[a] School of Chemistry and Chemical Engineering, Qilu University of Technology (Shandong Academy of Sciences), Ji'nan 250353, China
[b] School of Earth and Environment, Anhui University of Science and Technology, Huainan 232001, China
[c] Hubei Key Laboratory of Novel Reactor and Green Chemical Technology, Key Laboratory for Green Chemical Process of Ministry of Education, School of Chemical Engineering and Pharmacy, Wuhan Institute of Technology, Wuhan 430072, China

ARTICLE INFO

Article history:
Received 7 December 2024
Revised 6 April 2025
Accepted 29 May 2025
Available online 29 May 2025

Keywords:
Photocatalysis
N_2O adsorption
Electron enrichment
Nitric oxide
Reduction

ABSTRACT

Photocatalysis shows promising application in efficient reduction of nitrogen oxides (NO_x). However, the sluggish selectivity in nitric oxide removal with reductants, resulting in the formation of undesired N_2O byproducts, presents a great challenge. In this work, complete prohibition of nitric oxide generation in photo-removal of NO with carbon particulate is successfully achieved through the rational regulation of electron-trapping centers on TiO_2 nanosheets (TNS) surface achieved by the surface reduction treatment with $NaBH_4$. The efficient suppression (100%) of N_2O generation is ascribed to the more stable N_2O adsorption on the active (001) crystalline plane of TNS and the electron-capturing ability around oxygen vacancies based on the density functional theory (DFT) and experimental investigations. The existence of O_2 and H_2O effectively promote the photocatalytic activity of NO reduction but demonstrate no adverse effect on N_2O suppression. The optimal photocatalytic NO reduction activity with the highest CO_2 formation rate of 5.54 mg g^{-1} h^{-1} without N_2O formation is achieved over the optimized 0.135-TNS. These investigations guide the development of feasible photocatalytic treatment of air pollutants, emphasizing the significance of managing electron capture and gas adsorption for efficient byproduct control in pollutants removal.

© 2025 Published by Elsevier B.V. on behalf of Chinese Chemical Society and Institute of Materia Medica, Chinese Academy of Medical Sciences.

Environmental and energy crisis is becoming much serious all over the world due to the rapid development of modern industry. Nitrogen oxides (NO_x) could be produced in fossil fuel combustion or high-temperature related industrial process such as vehicle exhaust gases, power plants, *etc.* [1]. Notably, NO_x are the dominant components of air pollutants which are responsible for the formation of photochemical smog or acid rain [2]. Utilization of photocatalysis for NO_x removal is one of the most promising technologies thanks to the mild reaction conditions [3–5]. However, the application of photocatalytic NO_x removal in practical conditions is still restricted by the low photocatalytic efficiency and release of toxic byproducts.

Photo-generated reactive oxygen species including hydroxyl radicals and superoxide radicals can be utilized for photocatalytic oxidation of NO_x, thereby producing soluble nitrates on the surface of photocatalysts [6]. Specific gas adsorption and optimized electronic structure of photocatalysts can be applied to improve nitric oxide oxidation activity and to avoid NO_2 formation [3,7]. The d orbitals or d/p hybrid orbitals of alkaline earth metals can be utilized as the transportation channels of electrons to activate water vapor and oxygen, thus forming abundant oxidizing species and effectively oxidizing NO into nitrates [8]. Nevertheless, photocatalysts deactivation because of the surface coverage of nitrates can occur during photocatalytic oxidation of nitric oxide, thereby necessitating periodic catalyst regeneration [9].

Photocatalytic reduction of NO_x into harmless N_2 is a promising approach for pollutant air treatment. Research on this method have been known to be reported on TiO_2-based materials. Nitric oxide can be photocatalytically converted into N_2 with 96% selectivity by NH_3 over TiO_2 with the formation of NH_2NO as intermediate *via* Eley-Rideal mechanism [10]. Even in the presence of oxygen, NO can be reduced to N_2 with NH_3 over TiO_2 nanotube arrays under light irradiation [11]. In addition, the improved light absorption ability and facilitated charge separation efficiency on g-C_3N_4/TiO_2 were found to significantly enhance the photocatalytic

* Corresponding authors.
E-mail addresses: rutingyuan@qlu.edu.cn (R. Yuan), gqzddup@163.com (G. Zhao), zwchem@hotmail.com (W. Zhou).
[1] These authors contributed equally to this work.

https://doi.org/10.1016/j.cclet.2025.111398
1001-8417/© 2025 Published by Elsevier B.V. on behalf of Chinese Chemical Society and Institute of Materia Medica, Chinese Academy of Medical Sciences.

reduction of NO by using CO as the reducing agent [12]. Byproduct N_2O can be formed during the process of NO dissociation which is the rate-determining step for photo-reduction of NO [12]. However, the addition of extra reducing agents such as NH_3 could lead to secondary pollution because of incomplete reaction. Martens group found that carbon particles, which is co-existed air pollutants in exhaust gases, can be utilized as reducing agents for photocatalytic nitric oxide reduction [13], even in the presence of molecular oxygen [14]. The photocatalytic efficiency of nitric oxide reduction with carbon can be effectively enhanced *via* the construction of Bi_2WO_6/TiO_2 heterojunctions [15]. Nitrogen dioxide can also be photocatalytically reduced by carbon particles in the presence of NH_2-UiO-66/TiO_2 nanocomposites [16]. However, N_2O is easily generated during the photocatalytic NO_x reduction process. Thus, efficient charge transfer and abundant photo-generated electrons are highly demanded for the inhibition of N_2O formation in the reduction process of NO [15].

Oxygen vacancies in TiO_2 can be used as electron trapping centers during photocatalytic reactions, thereby increasing the concentration of photo-generated electrons around active centers [17]. Oxygen vacancies in TiO_2 present a critical part in actively promoting the photocatalytic activity for various reactions including photocatalytic CO_2 reduction [17], water splitting [18], VOCs degradation [19], NO oxidation [20], *etc.* However, oxygen deficiency detected in anatase TiO_2 nanosheets is at a negligible level by direct synthetic procedures [21,22]. To our knowledge, the role of oxygen vacancies on TiO_2 nanosheets surface have not yet been investigated for the N_2O inhibition during photocatalytic NO reduction with co-existed pollutants (carbon particles).

Herein, we present complete prohibition of byproduct formation *via* the combination of accumulated electrons and enhanced N_2O adsorption around active sites during NO_x photo-removal by soot particulates over TiO_2 nanosheets with tunable oxygen vacancies. The density functional theory (DFT) proves that the byproduct N_2O is more strongly adsorbed on oxygen deficient TiO_2 (001) crystalline facet where the photo-induced e^- can be effectively captured and enriched by oxygen defects, thus leading to completely reduction of N_2O. 0.135-TNS achieved the optimal photocatalytic NO reduction activity with the highest CO_2 formation rate of 5.54 mg g^{-1} h^{-1} without N_2O formation. This work may open new perspective for the suppression of byproduct formation in efficient NO_x photo-reduction process.

Surface oxygen deficiencies of TNS are supposed to be generated due to the reduction process. After the reduction by $NaBH_4$, the color of the TNS sample obviously changed from white to grey (Fig. S1 in Supporting information), indicating that the light utilization ability of TNS can be improved after the reduction treatment [23]. Scanning electron microscopy (SEM) and high-resolution transmission electron microscopy (HRTEM) images for the original TNS and 0.135-TNS are displayed in Fig. 1 and Fig. S2 (Supporting information). As shown in Fig. S2a, the pristine TNS has a rectangle morphology with width of 50–200 nm and thickness of *ca.* 5 nanometers. After the $NaBH_4$ treatment, the edges and surfaces of TNS sample turned into vague and rough with decreased dimensions (Fig. S2b). The TNS tended to stack together after surface reduction treatment, leading to more exposure of the edges than pristine TNS (Figs. S2a and b in Supporting information). HRTEM of the pristine TNS (Fig. 1b) and the 0.135-TNS (Fig. 1d) indicate that the lattice distance of the crystal plane is approximately 0.237 nm. Combining with X-ray diffraction (XRD) results, this spacing is attributed to the (001) plane of the anatase TiO_2. The (001) plane is more reactive than the (101) plane, due to the high surface energy, which is desirable for chemical reactions [24].

The XRD patterns of the pristine and defective TNS samples (0.015-TNS, 0.045-TNS, 0.09-TNS, 0.135-TNS, 0.18-TNS) are presented in Fig. S3a (Supporting information). Anatase phase was detected in the synthesized samples (JCPDS card No. 21–1272) [25]. XRD patterns of the pristine and reduced TNS are almost identical. a little decreased diffraction intensity and an increased half-peak breadth of (101) peak along with incremental content of the $NaBH_4$ indicate that part of Ti^{4+} could be reduced to Ti^{3+}. These observations could also be attributed to the increased amount of oxygen deficiencies in the reductant process, leading to slightly lattice disorder. The light utilization abilities of the TNS and 0.135-TNS photocatalysts were investigated through UV–vis diffuse reflection spectroscopy (Fig. S3b in Supporting information). The bandgaps were estimated by Tauc plots (Fig. S3c in Supporting information) [26]. Since anatase TiO_2 is an indirect semiconductor, the coefficient η of TiO_2 is 4 [27]. The band gap of TNS and 0.135-TNS is determined to be 3.2 eV and 3.05 eV, respectively with the correction of baselines for indirect semiconductors [28]. Mott-Schottky curves (Fig. S3g in Supporting information) suggested that the conduction band values are −0.32 V for the pristine TNS and −0.43 V for the 0.135-TNS because the flat band potential of anatase TiO_2 is very close to the corresponding conduction band minimum [29]. Combined the UV–vis analyses and Mott-Schottky measurements, the valence band changed from 2.88 V for pristine TNS to 2.62 V for 0.135-TNS which is obtained *via* the equation ($E_g = E_{VB} - E_{CB}$).

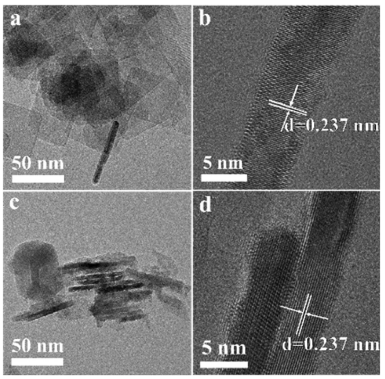


Fig. 1. (a, b) HRTEM images of the pristine TiO_2 nanosheets and (c, d) the defective TiO_2 nanosheets (0.135-TNS).

The chemical states of different elements in TiO_2 before and after surface reduction were investigated by XPS spectra, as demonstrated in Figs. S3d-f (Supporting information). The obtained XPS spectra were adjusted with the reference of C 1s at 285.8 eV. The XPS survey spectra are presented in Fig. S3d, whilst the high-resolution XPS spectra of Ti and O are illustrated in Figs. S3e and f, respectively. No XPS spectra of carbon or F was obtained during the measurement, suggesting the complete removal of organic matter or fluoride anions from the TNS. The O 1s spectra exhibits two peaks in Fig. S3e. The binding energy at 529.9 eV is attributed to oxygen band of Ti-O-Ti [30]. The peak centered at 532.0 eV is ascribed to the O-atoms beside the oxygen deficiencies [31,32]. For the 0.135-TNS, Ti-O-Ti bond shifted to higher binding energy of 530.3 eV. Moreover, binding energy of 532.0 eV for 0.135-TNS is much greater than that of the pristine one, confirming the increased oxygen vacancy concentration after reducing treatment [19]. Ti 2p XPS spectra show four main binding energies in Fig. S3f. The measured binding energy of Ti^{4+} state in the pristine TNS is 458.8 eV for Ti $2p_{3/2}$ and 464.4 eV for Ti $2p_{1/2}$ [33]. Compared with the pristine TNS, the two peaks shifted ∼0.3 eV to higher binding energies for the 0.135-TNS. Additionally, two detectable shoulder peaks can be found at 460.1 eV and 457.6 eV for 0.135-TNS, which are corresponding to the Ti^{3+}species, suggesting that Ti^{3+} species were produced during the synthesis [34]. The existence of oxygen deficiencies was further studied by electron paramagnetic resonance (EPR) in Fig. S3h (Supporting information). The 0.135-TNS

sample presents a sharp peak at $g = 2.003$, thus proving the successful creation of oxygen deficiencies [35]. It demonstrates almost no signal for the pristine one. Although the TNS and 0.135-TNS were almost nonporous according to the isothermal curves, the stacking sheets could generate intra-crystalline pores. The 0.135-TNS exhibits wider pore size distribution with average pore size increased from 38 nm to 84 nm after $NaBH_4$ treatment, as demonstrated in Fig. S3i (Supporting information). This may be caused by the dissolution of the edge of TiO_2 crystals. The generated large pores would be beneficial for the transfer of gas reagents and intermediate products, thereby resulting in high catalytic reactivity.

Photo-removal of nitric oxide with carbon particles (Printex U) under mild ambient condition was conducted in a homemade reactor set-up with a gas supply system. Printex U from Evonik is a typical carbon black material for carbon oxidation research and is hard to be oxidized. Reactions under varied conditions were performed in batch mode since the amounts of yielded gaseous compounds were too low to be detected by gas analyzers (about 1 ppm) under continuous gas flow conditions. The volumetric hourly space velocity (VHSV) was determined to be 187.5 h^{-1}. The contact time of NO with defective TNS is *ca.* 0.32 min under gas flow conditions. No carbon monoxide or carbon dioxide generation was detected utilizing carbon particles without TNS under light illumination and in reactions in the absence of light with TNS and carbon. No nitric oxide adsorption by Printex U was observed during the control experiments. Gas product (N_2, NO_2, N_2O) distribution after 210 min reaction over pristine TNS and x-TNS is shown in Fig. 2a (x is the weights of $NaBH_4$). 12 % N_2O was formed in the presence of the pristine TNS. In comparison with the pristine TNS, N_2O formation can be suppressed at different degrees using x-TNS. Utilizing the 0.015-TNS, 0.045-TNS, 0.09-TNS and 0.18-TNS as the photocatalysts in the photocatalytic reduction of NO, N_2O selectivity decreased from 12 % to 9.0 %, 6.3 %, 4.0 %, and 10.7 %, respectively, compared with pristine TNS (Table S1 in Supporting information). Besides N_2O, NO_2 formation was also inhibited in the presence of defective TNS. Notably, no N_2O was formed by using 0.135-TNS as photocatalyst, leading to 100 % N_2 selectivity (Table S2 in Supporting information). These results indicate that oxygen vacancies in TNS samples have a positive effect on inhibiting N_2O formation in NO photo-reduction with carbon. The introduction of oxygen defects on TNS could facilitate charge separation and migration efficiency under light illumination [36]. However, excessive amounts of oxygen deficiencies on 0.18-TNS could lead to the bulk defects which could prohibit the transfer of electrons to the surfaces of TNS [18], thereby leading to higher N_2O formation than 0.135-TNS (Fig. 2a, Table S1). The effect of varied ratio between 0.135-TNS and carbon particles on photocatalytic nitric reduction has been investigated and concluded in Table S3 (Supporting information). The nitric oxide conversion and N_2 selectivity (100 %) were not affected by changing the amount of carbon particles while CO_2 formation was slightly influenced. This is because the nitric oxide concentration is relatively low in the presence of plenty of carbon particles. The CO_2 generation slightly decreased when the amount of carbon particles was reduced from 5 mg to 2.5 mg or increased to 7.5 mg. The presence of excessive carbon particles could lead to the coverage of active sites of TNS, thereby lowering the light absorption and photocatalytic activity.

The CO_2 formation in nitric oxide photo-reduction with carbon by 0.135-TNS was significantly increased compared with the pristine TNS, as shown in Fig. 2b. The highest CO_2 formation rate of 5.54 mg g^{-1} h^{-1} was achieved over 0.135-TNS surface, which is approximately 1.6 times that of pristine TNS. In addition, the 0.135-TNS sample showed a steady photocatalytic performance, whilst the carbon removal rate for pristine TNS significantly declined at the third illumination period. Carbon monoxide generation was marginally increased over 0.135-TNS (Table S2), because CO could be the intermediate product in the formation of CO_2. N_2O was not detected during all the illumination periods. 100 % NO conversion was reached during the reactions with 100 % N_2 selectivity.

The influence of gaseous H_2O on nitric oxide photo-reduction with carbon was also investigated with the existence of 1000 ppm NO and 5 % O_2 with or without 3 % H_2O, as illustrated in Fig. 2c and Table S2. The existence of water vapor demonstrated positive effect on photocatalytic activity for NO reduction using the 0.135-TNS as photocatalyst. In the first and second illumination period, CO_2 formation was almost doubled. In the last illumination, CO_2 formation was enhanced 1.5 times to that without water vapor. N_2O was not detected w/o the addition of water vapor in all reactions, indicating the N_2O suppression activity of 0.135-TNS was little influenced by water vapor. The nitric oxide photo-removal activity over 0.135-TNS was also studied with different amount of NO (Fig. S4, Table S4 in Supporting information). The CO generation slightly elevated with nitric oxide concentrations. The overall CO_2 generation in 210 min reaction with the existence of 300, 500, and 1000 ppm NO with 5 % O_2 reached 19.89, 20.56, 21.84 μmol, respectively. There is NO, NO_2, or N_2O formation in these experiments, suggesting the complete NO reduction with efficient N_2O inhibition even in the presence of oxygen.

A 66 h reaction with seven continuous irradiation durations was conducted over 0.135-TNS to investigated the corresponding photocatalytic stability (Fig. 2d). It is obviously noticed that the CO_2 generation activity in the beginning two irradiation durations is higher than the follow irradiations. As previously documented, Printex U, which is typical material for carbon removal reactions, contains complicated compositions with oxygenated components (easy carbon) and refractory carbon [14,15]. The 'easy carbon' such as C–O–C is easy to be photocatalytically removed at the early stage of the long-term reaction. Afterwards, the refractory part could be gradually activated and oxidized by photo-generated oxidizing species such as $^{\bullet}OH$ and $^{\bullet}O_2^-$. Moreover, N_2O was not formed during the seven consecutive photocatalytic NO reduction processes, as presented in Table S5 (Supporting information). 100 % NO conversion with 100 % N_2 selectivity in the long-term reaction was achieved, further proving the byproduct inhibition due to the presence of oxygen vacancies on 0.135-TNS, as illustrated in Table S5.

The highest nitric oxide conversion efficiency was compared with recently reported photocatalysts, as presented and listed in Fig. 2e and Table S6 (Supporting information). Currently, most photocatalysts have been investigated for the oxidation of nitric oxide, thereby leading to the formation of nitrates as the final product which is harmful for the environment. Notably, N_2 is the main product in this study. Among the reported high-activity photocatalysts for nitric oxide removal, such as element modified TiO_2, carbon nitride, layered double hydroxides (LDHs), and photocatalyst composites, 0.135-TNS demonstrates the best nitric oxide removal efficiency (100 %) with the highest N_2 selectivity (100 %) in spite of the highest concentration of nitric oxide (1000 ppm). However, the coverage of soot particle on the surface of photocatalysts could lead to catalyst deactivation under practical conditions. Further research is currently conducted on the optimization of reaction conditions for practical utilization.

To investigate the migration and recombination process of the photo-generated charges in TNS and 0.135-TNS, photoluminescence (PL) spectra measurements were conducted. As shown in Fig. 2f, because of the existence of oxygen deficiencies on the surface, 0.135-TNS exhibited lower PL intensity, indicating lower charge recombination [37,38]. In addition, the electrochemical impedance (EIS) measurements (Fig. S5a in Supporting information) present that 0.135-TNS had a much lower interface resistance than pristine TNS. During the transient photocurrent measurements, 0.135-TNS demonstrated much higher photocurrent density than pristine TNS (Fig. S5b in Supporting information). The above measurements

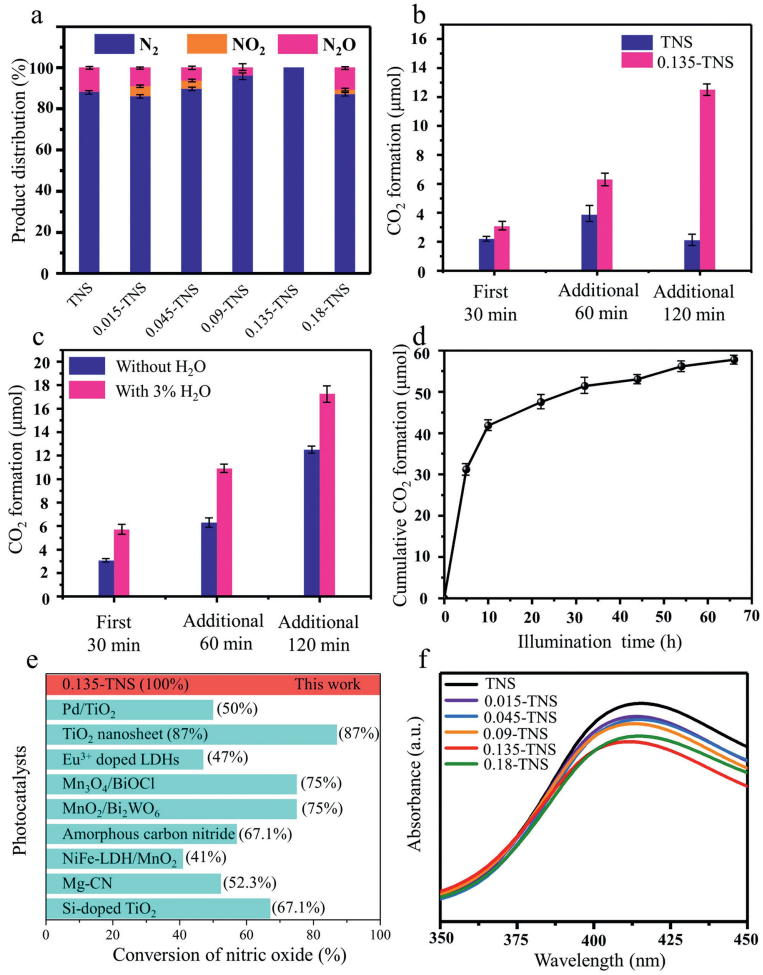


Fig. 2. (a) Product distribution in 210 min NO_x photo-reduction with carbon over pristine TNS and x-TNS at room temperature (x representing the amount of $NaBH_4$, gas composition: 1000 ppm NO, 5 % O_2). (b) CO_2 generation in NO photo-reduction by carbon over TNS or 0.135-TNS at room temperature (gas composition: 1000 ppm NO, 5 % O_2). (c) CO_2 generation in NO photo-reduction by carbon over 0.135-TNS at room temperature (gas composition: 1000 ppm NO and 5 % O_2 w/o 3 % H_2O). (d) Cumulative CO_2 generation in long-term NO photo-reduction with carbon particles over 0.135-TNS (gas composition: 1000 ppm NO, 5 % O_2 and 3 % H_2O). (e) Comparison of nitric oxide removal efficiency with several reported photocatalysts. (f) Photoluminescence (PL) spectra of different photocatalysts, excitation wavelength: 240 nm.

proved that the charge separation and migration efficacy of TNS was significantly improved upon the introduction of oxygen vacancies [39]. The suppression of photo-carriers recombination can effectively facilitate the electron migration efficiency and the subsequent photo-reduction stage, which is inconsistent with the catalytic performance in photocatalytic NO reduction by carbon particulates. The solid products formed on TNS surface during photocatalytic NO reduction with carbon were investigated by FTIR spectra, as illustrated in Fig. 3a. Compared to the fresh 0.135-TNS photocatalysts, the absorption at 1384 cm^{-1} emerged, which can be attributed to nitrate generation on TNS surface [40]. The nitrate generation and decomposition is certified to be a dynamic equilibrium in previously reported research [14]. Nitrates can be consumed through the reduction of nitrates by NO on TiO_2 surface. Based on the CO_2 generation and NO_x removal data among all illumination periods, the dynamic nitrate generation has little influence on the photocatalytic activity of 0.135-TNS.

To gain insight into the influence of oxygen defects on the charge distribution of TNS surface, DFT calculations based on differential charge density were applied, as shown in Fig. 3b. From the top view of the differential charge density distribution image, the sites around oxygen defect exhibited higher charge density distribution than other parts. This charge redistribution and localization makes the charge separation more efficient. In addition, Fig. 3b suggests that the defective TNS surface can create electron-rich region around oxygen vacancies which can act electron reservoir under light irradiation [41], indicating more electrons are concentrated on defective TNS surface for NO_x reduction. According to DFT calculations, the work function of TNS could be tuned to further enhance the charge separation efficiency, as presented in Figs. 3c and d. The work function upper of defective TNS (3.931 eV) is much lower than the TNS without oxygen defects (6.050 eV), thereby suggesting electron flow from defective TNS surface to reactants can more easily occur to enable the further reduction of reaction intermediate N_2O to nitrogen.

As described above, up to 19 % N_2O can be formed during photocatalytic reduction of NO with carbon particles over pristine TNS (Table S2). Similarly, relatively high amounts of N_2O (up to 35 % selectivity) was also generated during the NO photo-reduction on the anatase TiO_2 nanoparticles surface in our previous research [13]. Notably, no N_2O formation with 100 % N_2 selectivity was achieved over the surface of 0.135-TNS with certain amounts of oxygen vacancies. In addition, N_2O was assumed to be generated during the reoxidation process of Ti^{3+} with NO instead of O_2 [42]. Thus, N_2O could be the intermediate species for the reduction of nitric oxide to nitrogen. To unravel the reaction mechanism behind efficient N_2O suppression during NO photo-removal by carbon particles on defective TNS surface, the DFT was applied. The optimized

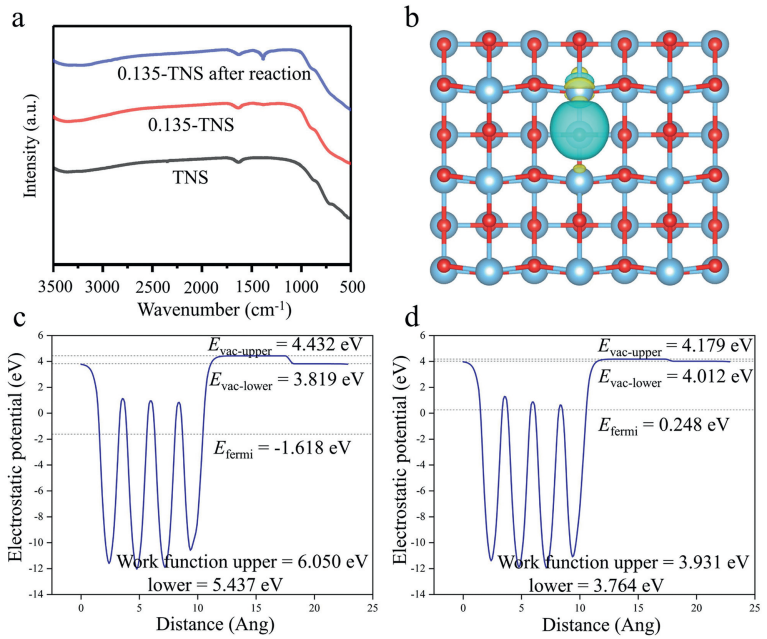


Fig. 3. (a) FTIR spectra of pristine TNS and 0.135-TNS before reaction, and 0.135-TNS after 210 min reaction (gas composition: 1000 ppm NO, 5% O_2 and 3% H_2O). (b) Differential charge density distribution (top view) on defective TNS with yellow and cyan isosurfaces representing charge gain and loss, respectively. Electrostatic potential of (c) anatase TiO_2 (001) without oxygen defects, and (d) anatase TiO_2 (001) with oxygen defects. The work function is the calculated difference between vacuum level and Fermi energy.

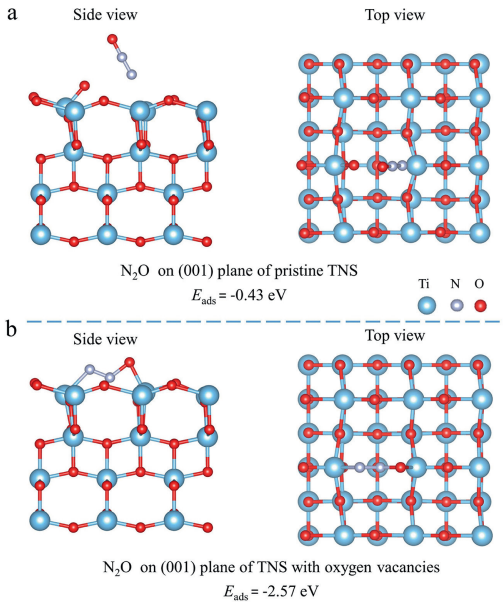


Fig. 4. DFT calculations for the adsorption energies of N_2O on the (001) crystalline plane of the pristine TNS (a), and TNS with oxygen vacancies (b), respectively.

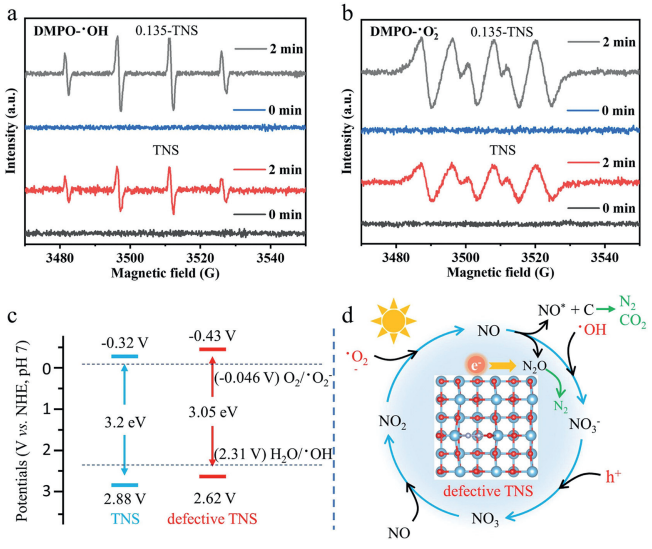


Fig. 5. ESR spectra in the different systems: (a) •OH, (b) $^{\bullet}O_2^-$ in the presence of TNS or 0.135-TNS under light illumination for 0 or 2 min. (c) Band alignment of TNS and defective TNS. (d) Proposed mechanism for photocatalytic NO reduction with carbon particles on defective TNS surface.

adsorption structure for N_2O adsorbed on TNS or defective TNS and the corresponding adsorption energies are illustrated in Fig. 4. As shown in the HR-TEM images, (001) crystalline plane was found to be the dominant exposed facet of TNS, which was supposed to be the active facet of anatase TiO_2 nanosheets [21]. The energy barriers of N_2O adsorption on (001) crystalline plane of TNS and defective TNS are determined to be −0.43 eV and −2.57 eV, respectively, as shown in Figs. 4a and b. It is obviously observed that the adsorption stability of N_2O on defective TNS is about 5.9 folds higher than pristine TNS, thus suggesting that the formed N_2O can be more easily and stably adsorbed on the (001) plane of defective TNS with oxygen vacancies than pristine TNS. Therefore, during photocatalytic NO reduction process, the generated N_2O can accumulate on the (001) crystalline plane of defective TNS easily and continuously. In the meantime, the photo-induced electrons can be continuously captured by the oxygen vacancies on the (001) plane of defective TNS since oxygen vacancies are supposed to be electron-trapping centers during photocatalytic reactions [43].

Electron spin resonance spectroscopy (ESR) was utilized to investigate the reactive oxygen species over TNS and 0.135-TNS (Figs. 5a and b). No reactive oxygen species were detected over the photocatalysts in the dark. Under light irradiation for 2 min, the ESR signals for hydroxyl radicals (•OH) and superoxide radicals ($^{\bullet}O_2^-$)

in the presence of both pristine TNS and 0.135-TNS were obviously observed. Notably, 0.135-TNS demonstrates much higher ESR signals for $^{\bullet}OH$ and $^{\bullet}O_2^-$ than pristine TNS, indicating the superior ability of 0.135-TNS for generating reactive oxygen species because of the presence of oxygen defects. According to the UV–vis spectra and Mott-Schottky measurements, the conduction band of TNS shifted from −0.32 V to −0.43 V (Fig. 5c) after the introduction of oxygen vacancies, indicating that the defective TNS have superior reduction ability [44]. Therefore, the further reduction of the intermediate N_2O into nitrogen on defective TNS surface occurred smoothly with the high concentration of accumulated photo-induced electrons, which in consistent with N_2O generation data in all conducted reactions. As shown in Fig. S6a (Supporting information), the possible reaction intermediates during photocatalytic NO reduction with carbon particles over 0.135-TNS were investigated by *in-situ* FTIR spectroscopy. During the photocatalytic process, the absorption around 1684 cm^{-1} attributed to NO_2 can be observed [45]. The absorption of nitrates around 1380 cm^{-1} is found to be present during the reaction. Nitric oxide accepted e^- to form NO^- (1174 cm^{-1}) was also observed [46]. Notably, N_2O (1250 cm^{-1}) on the catalyst surface accumulated in the first several minutes, then gradually disappeared during the reaction [47]. After the introduction of oxygen vacancies in TNS, the surface adsorption of NO on TNS was enhanced according to Fig. S6b (Supporting information), thereby facilitating the subsequent reduction reaction. In addition, the calculated free energy suggested that the generation of target product N_2 from NO or N_2O conversion were thermodynamically accelerated on defective TNS with oxygen vacancies. As shown in Fig. 5d, under light illumination, nitric oxide could be activated by photogenerated electrons over 0.135-TNS to form the possible reaction intermediates NO^* which could attack carbon particles to generate N_2 and byproduct N_2O with corresponding CO_2 formation [15]. However, because of the limited characterization techniques, the possible intermediates NO^* have not been confirmed yet. Future research is currently investigated to tackle this problem. The formed N_2O could be steadily adsorbed on (001) crystal plane of defective TNS and subsequently be reduced to N_2 by the enriched concentration of electrons around oxygen vacancies. In the meantime, nitric oxide could be attacked by $^{\bullet}OH$ to NO_3^- [48]. Also, the reaction of NO with oxygen can form NO_2 which could react with $^{\bullet}OH$ to generate HNO_3 [15]. In the presence of photo-generated $^{\bullet}OH$ and $^{\bullet}O_2^-$ on TNS surface, the generation and decomposition of nitrates can finally reach a dynamic equilibrium [48]. The proposed reactions over 0.135-TNS under light irradiation are listed below (Eqs. 1–9):

$$0.135\text{-TNS} + h\nu \rightarrow e^- + h^+ \quad (1)$$

$$O_2 + e^- \rightarrow {}^{\bullet}O_2^- \quad (2)$$

$$H_2O + h^+ \rightarrow {}^{\bullet}OH + H^+ \quad (3)$$

$$NO + e^- \rightarrow NO^* + C \rightarrow N_2 + N_2O + CO_2 \quad (4)$$

$$N_2O + e^- + 2H^+ \rightarrow N_2 + H_2O \quad (5)$$

$$NO + {}^{\bullet}OH \rightarrow NO_3^- + H^+ \quad (6)$$

$$NO_3^- + h^+ \rightarrow NO_3 \quad (7)$$

$$NO_3 + NO \rightarrow NO_2 \quad (8)$$

$$3NO_2 + {}^{\bullet}O_2^- \rightarrow NO + 2NO_3^- \quad (9)$$

We utilized oxygen vacancies on TNS surface to create electron-trapping centers and N_2O adsorption sites to achieve the objective of this study: efficient prohibition of N_2O formation during much improved photocatalytic nitric oxide reduction process. N_2O generation has been effectively prohibited during photocatalytic reduction of NO with carbon particles *via* rational regulation of oxygen deficiencies on titanium dioxide nanosheets surface. The presence of oxygen presented no negative influence on the inhibition of N_2O formation. The addition of water vapor can effectively enhance the redox reaction rate with no promotion effect on N_2O generation. Density functional theory calculations directed understanding of the efficient prohibition of N_2O formation in NO–C redox reaction to the combination of stable adsorption of N_2O on defective TNS surface and enriched amounts of photo-induced e^- captured by oxygen vacancies as the electron-trapping centers. The optimized 0.135-TNS exhibited the highest activity for NO photo-removal by carbon particulates and 100 % N_2O inhibition during reactions under varied conditions. However, the photocatalytic NO reduction efficiency is too low to be applied in practical conditions. Strategies for improving the photocatalytic efficiency including the combination of photo- and thermo-catalysis, construction of heterojunctions are highly demanded. Nevertheless, this work provides alternative strategy for toxic byproduct suppression during NO_x photo-removal process, thereby demonstrate significant potential for air pollutants control.

Declaration of competing interest

The authors declare that they have no known competing financial interests or personal relationships that could have appeared to influence the work reported in this paper.

CRediT authorship contribution statement

Lijun Liao: Writing – original draft, Investigation, Formal analysis, Data curation, Conceptualization. **Yuhao Wang:** Writing – original draft, Methodology, Investigation, Data curation. **Yanbo Li:** Validation, Investigation, Formal analysis. **Yingchun Chen:** Methodology, Formal analysis, Data curation. **Ruting Yuan:** Writing – review & editing, Supervision, Investigation, Formal analysis. **Bo Wang:** Software, Methodology, Formal analysis. **Tiancheng Zhuang:** Validation, Software, Data curation. **Guangquan Zhao:** Writing – review & editing, Investigation, Formal analysis, Data curation. **Wei Zhou:** Writing – review & editing, Supervision, Project administration, Investigation.

Acknowledgments

We gratefully acknowledge the support of the National Natural Science Foundation of China (No. 52172206), the Shandong Provincial Natural Science Foundation (Nos. ZR2022QD062 and ZR2023QD036), the Open Project of Key Laboratory of Green Chemical Engineering Process of Ministry of Education (No. GCP2023003), Science, Education and Industry Integration Innovation Pilot Project from Qilu University of Technology (Shandong Academy of Sciences) (No. 2024ZDZX13), the Talent Research project of Qilu University and Technology (Shandong Academy of Sciences) (Nos. 2024RCKY018, 2024RCKY036 and 2023RCKY083), and the State Key Laboratory of Heavy Oil Processing, China University of Petroleum (No. SKLHOP202402009).

Supplementary materials

Supplementary material associated with this article can be found, in the online version, at doi:10.1016/j.cclet.2025.111398.

References

[1] Y.K. Park, B.S. Kim, Chem. Eng. J. 461 (2023) 141958.
[2] J. Li, T. Chen, H. Zhang, et al., Sci. Total Environ. 912 (2024) 168333.
[3] J. Zhao, S. Li, R. Liang, et al., Appl. Catal. B: Environ. Energy 352 (2024) 123982.
[4] W. Dai, S. Zhang, H. Shang, et al., Adv. Funct. Mater. 34 (2024) 2309426.
[5] J. Liu, X. Huang, L. Jia, et al., Small 19 (2023) 2207198.
[6] T. Xue, J. Li, L. Chen, et al., Chem. Sci. 15 (2024) 9026–9046.
[7] J. Liu, X. Huang, L. Hu, et al., Chem. Eng. J. 476 (2023) 146768.
[8] W. Zhang, H. Bai, B. Ma, et al., Appl. Catal. B: Environ. Energy 356 (2024) 124241.
[9] N. Li, C. Wang, K. Zhang, et al., Chin. J. Catal. 43 (2022) 2363–2387.
[10] K. Teramura, T. Tanaka, S. Yamazoe, K. Arakaki, T. Funabiki, Appl. Catal. B: Environ. 53 (2004) 29–36.
[11] Y.C. Chou, Y. Ku, Chem. Eng. J. 225 (2013) 734–743.
[12] Y. Ren, Q. Han, J. Yang, et al., J. Colloid Interface Sci. 610 (2022) 152–163.
[13] L. Liao, S. Heylen, B. Vallaey, et al., Appl. Catal. B: Environ. 166-167 (2015) 374–380.
[14] L. Liao, S. Heylen, S.P. Sree, et al., Appl. Catal. B: Environ. 202 (2017) 381–387.
[15] R. Yuan, M. Wang, L. Liao, et al., Chem. Eng. J. 453 (2023) 139892.
[16] Y. Liu, L. Liao, L. Guo, et al., Environ. Res. 240 (2024) 117515.
[17] J. Li, M. Zhang, Z. Guan, et al., Appl. Catal. B: Environ. 206 (2017) 300–307.
[18] Y. Zhang, Z. Xu, G. Li, et al., Angew. Chem. Int. Ed. 58 (2019) 14229–14233.
[19] Y. Wang, Y. Zhang, X. zhu, Y. Liu, Z. Wu, Appl. Catal. B: Environ. 316 (2022) 121610.
[20] X. Bi, G. Du, A. Kalam, et al., Chem. Eng. Sci. 234 (2021) 116440.
[21] H.G. Yang, G. Liu, S.Z. Qiao, et al., J. Am. Chem. Soc. 131 (2009) 4078–4083.
[22] H.G. Yang, C.H. Sun, S.Z. Qiao, et al., Nature 453 (2008) 638–641.
[23] Y. Zhang, J. Yan, Chem. Eng. J. 472 (2023) 144831.
[24] W.Q. Fang, J.Z. Zhou, J. Liu, et al., Chem. Eur. J. 17 (2011) 1423–1427.
[25] Y. Dai, C.M. Cobley, J. Zeng, Y. Sun, Y. Xia, Nano Lett. 9 (2009) 2455–2459.
[26] M. Wang, S. Wang, Z. Li, et al., J. Photochem. Photobiol. A: Chem. 455 (2024) 115754.
[27] W. Navarra, I. Ritacco, O. Sacco, et al., J. Phys. Chem. C 126 (2022) 7000–7011.
[28] P.H.M. Andrade, C. Volkringer, T. Loiseau, et al., Appl. Mater. Today 37 (2024) 102094.
[29] X. Yang, F. Li, W. Liu, et al., Appl. Catal. B: Environ. 324 (2023) 122202.
[30] A.S. Eltaweil, N. Al Harby, A.I. Osman, et al., J. Ind. Eng. Chem. 143 (2025) 704–716.
[31] J. Wan, W. Chen, C. Jia, et al., Adv. Mater. 30 (2018) 1705369.
[32] W. Zhang, H. He, Y. Tian, et al., Nano Energy 66 (2019) 104113.
[33] S. Cheng, Y.J. Gao, Y.L. Yan, et al., J. Energy Chem. 39 (2019) 144–151.
[34] X. Yu, X. Fan, L. An, et al., Carbon 128 (2018) 21–30.
[35] C. Zhao, Y. Yang, L. Luo, et al., Sci. Total Environ. 747 (2020) 141533.
[36] J. Liu, S. Li, Z. Qiu, et al., Small 19 (2023) 2300737.
[37] Z. He, H. Yang, N.H. Wong, et al., Small 19 (2023) 2207370.
[38] D. Liu, B. Sun, S. Bai, T. Gao, G. Zhou, Chin. J. Catal. 50 (2023) 273–283.
[39] Z. Li, T. Gao, H. Chu, et al., Appl. Catal. B: Environ. Energy 358 (2024) 124370.
[40] J. Ding, C. Yu, J. Lu, et al., Appl. Energy 263 (2020) 114681.
[41] M. He, Y. Cao, J. Ji, K. Li, H. Huang, J. Catal. 396 (2021) 122–135.
[42] K. Teramura, T. Tanaka, T. Funabiki, Langmuir 19 (2003) 1209–1214.
[43] M. Li, P. Wang, Z. Ji, et al., Appl. Catal. B: Environ. 289 (2021) 120020.
[44] X. Li, G. Fang, X. Qian, Q. Tian, Chem. Eng. J. 428 (2022) 131052.
[45] A. Mahmood, X. Wang, X. Xie, J. Sun, Colloids Surf. A: Physicochem. Eng. Asp. 626 (2021) 127058.
[46] W. Zhang, Y. Ma, C. Song, et al., Adv. Funct. Mater. 34 (2024) 2410902.
[47] L. Mino, M. Cazzaniga, F. Moriggi, M. Ceotto, J. Phys. Chem. C 127 (2023) 437–449.
[48] C.F. Sid Devahasdin Jr., Kuyen Li, D.H. Chen, J. Photochem. Photobiol. A: Chem. 156 (2003) 161–170.